A numerical study into effects of soil compaction and heat storage on thermal performance of a Horizontal Ground Heat Exchanger

F. Tang, M. Lahoori, H. Nowamooz, S. Rosin-Paumier, F. Masrouri

A numerical study into effects of soil compaction and heat storage on thermal performance of a Horizontal Ground Heat Exchanger

F. Tang[a,c], M. Lahoori [b], H. Nowamooz [a], S.Rosin-Paumier[b], F.Masrouri[b]

[a] *ICUBE, UMR 7357, CNRS, INSA de Strasbourg, 24 boulevard de la Victoire, 67084 Strasbourg*

[b] *LEMTA – CNRS UMR 7563, Université de Lorraine, Vandoeuvre-lès-Nancy F-54500, France*

[c] *School of Transportation Science and Engineering, Harbin Institute of Technology, Harbin 150090, China*

Email:

fujiao.tang@insa-strasbourg.fr

mojdeh.Lahoori@univ-lorraine.fr

hossein.nowamooz@insa-strasbourg.fr

sandrine.rosin@univ-lorraine.fr

farimah.masrouri@univ-lorraine.fr

Corresponding author: Mojdeh Lahoori (mojdeh.Lahoori@univ-lorraine.fr, sandrine.rosin@univ-lorraine.fr)

Abstract

The good capacity of the numerical simulations makes possible to bring some further responses on the backfill soil selection and its installation depth in the Horizontal Ground Heat Exchanger (HGHE). Therefore, a well-known backfill soil was considered to be used as substitutive material. The hydrothermal properties of the backfill material were estimated in laboratory and then injected in a numerical framework considering the atmosphere-soil-HGHE interaction. Numerical simulations were performed for a HGHE installed in the compacted backfill soil and the local natural soil. The simulation results showed that the compacted backfill soil improves by 8.5% the HGHE performance compared to local uncompacted soil. Two heat storage scenarios at three different installation depths were also investigated. The results showed that an inlet fluid temperature of 50 ^oC in summer increased highly the system performance by 13.7% to 41.4%, while the improvement was less significant (0% to 4.8%) for the ambient inlet temperature scenario. A deeper installation depth of HGHE increased also the system performance, the more energy could be stored and extracted.

Keywords: Horizontal Ground Heat Exchanger; Numerical simulations; Atmosphere-soil-HGHE interaction; Backfill soil; Installation depth; HGHE Performance.

1 Introduction

Shallow geothermal energy is one of the many sources of renewable energy, and it can be easily accessed all around the world (H Abedin and A Rosen 2011; Shortall et al. 2015; Sangi and Müller 2018). The temperature of the ground can be exploited during winter using a ground source heat pump for space heating and during summer for cooling needs. To increase the efficiency of shallow geothermal energy the solar energy can be stored during summer to increase the temperature of the ground (Xu et al. 2014; Lee et al. 2018; Lahoori, Jannot, Rosin-Paumier, Boukelia and Masrouri 2020). Generally, open and closed heat exchangers are available for the exploitation of shallow geothermal energy (Florides and Kalogirou 2007), which are then served as low-potential sources of thermal energy for heat pumps (Adamovsky et al. 2015). Horizontal Ground Heat Exchanger (HGHE) is one of those closed loop heat exchangers. Compared to Vertical Ground Heat Exchanger (VGHE), it is more cost effective although it requires more installation space (Self et al. 2013).

Due to the shallow installation depth (conventionally between 1.0 and 2.0 m), HGHE is also more sensitive to the meteorological condition (Gonzalez et al. 2012; Habibi and Hakkaki-Fard 2018). The experimental investigations showed that the thermal performance depends on the depth of HGHE installation (Beier and Holloway 2015). At deeper position, the soil thermal properties are not affected by the daily and seasonally ambient temperature variation. The results reported by Elminshawy et al. (2017) showed that the thermal performance of the horizontal system highly depends on the soil compaction state (water content and density) and air flow rate. By increasing density, the solid particles are better packed into a unit volume and the number of contact points between the particles increases (Penner et al. 1975; Abu-Hamdeh and Reeder 2000). These contact points provide a larger heat transfer by conduction which causes the temperature variation between the inlet and outlet airflow. These observations are in agreement with the study of Hurtado et al. (2012) which investigated the capacity of a compacted soil to store thermal energy from the chimney power plant using an analytical model based on a finite volume procedure. They mentioned that the output power energy was increased by 10%

when the soil compaction increased from loose to dense level.

Since the experimental investigations are time and money consuming, the thermal performance of horizontal heat exchanger loops in soils has been numerically investigated using finite element and finite difference tools in different studies. Normally in these models, the simulation is done by considering a homogeneous soil mass with constant thermal properties and the heat transfer is modeled by conduction using solid particles of soil (Jradi et al. 2017). However, in unsaturated compacted soils, the thermal properties will change by temperature variations, soil physical and hydraulic properties. Therefore, a comprehensive investigation is a thermo-hydraulic simulation with consideration of the mass transfer by vapor and liquid flows (Gan 2013; Gao et al. 2016; Boukelia 2016; Li et al. 2018; Li et al. 2018). Asgari et al. (2020) showed that the thermal performance of the linear and slinky types of HGHE increases by increasing the number of layers arrangement in the ground. For the spiral type exchangers, the thermal performance did not change with increasing the number of layers. Boukelia (2016) investigated the heat lost in a seasonal storage system in an embankment using HGHE by conducting the coupled thermo-hydraulic numerical simulations with a finite element tool (Code-Bright). The author observed that when the inlet temperature in the HGHE during summer was 50 ^oC, the temperature of the soil close to the probes reached 38 ^oC. At the end of the autumn when the thermal extraction season started, the temperature was about 25 ^oC, therefore, about 13 ^oC of heat loss has been occurred. Jradi et al. (2017) showed the efficiency of the Air Source Heat Pump (ASHP) combined with a solar power system as a basis for seasonal thermal energy storage. They showed also that a huge heat loss occurred after storage seasons. Therefore, to increase the thermal performance of a medium to store thermal energy, the insulation material covering the soil might be a good option and it can be taken into account in the design stage (Lahoori, Rosin-Paumier, Stoltz and Jannot 2020).

Another challenging issue is the consideration of the atmosphere-soil-HGHE interaction in the prediction of the system performance. Tang and Nowamooz (2020) proposed a numerical simulation framework to evaluate the HGHE performance in field conditions

by considering energy and water balance on the land surface. They showed in their simulations that the consideration of the atmosphere-soil-HGHE interaction underestimates highly the outlet temperature especially for the horizontal systems installed close to the soil surface up to a difference of 48%.

The good capacity of the numerical framework considering the atmosphere-soil-HGHE interaction makes possible to bring some further responses on the backfill soil characteristics and the installation depth rarely studied so far. This point is very crucial for the thermal performance of the horizontal systems. Modeling the soil characteristics such as the compaction state and thermal properties may significantly improve the system performance, and also avoid the cost of HGHE installation at deeper depths.

In this context, the investigation aims to visualize how the compacted backfill soil would influence the HGHE performance. In addition, two energy storage scenarios are compared at different installation depths, giving a highlight on how the installation depth would influence the energy storage applications in HGHE. Therefore, a compacted backfill soil which hydric and thermal properties have been measured in laboratory, is considered. Then, hydrothermal properties of the compacted soil are estimated and embedded in the numerical framework considering the atmosphere-soil-HGHE interaction.

2 Hydrothermal behavior of the studied soil

The studied soil is frequently used as the backfill soil in France. The material was classified as sandy lean clay, CL, according to the Unified Soil Classification System (ASTM 2000). Regarding the X-ray diffractograms analysis the compacted soil contains 81% quartz, 7% dolomite, 5% calcite, 5% clayey materials and 3% feldspar. According to the particle-size distribution, almost 20% of the particles of the soil were smaller than 2 μm corresponding to the clay content, and 59% were higher than 0.05 mm corresponding to the sand content (x_s). With a liquid limit (LL) of 27% and a plastic limit (PL) of 21%, the plasticity index (PI) was 6%. The backfill soil is compacted at a water content of 16.3% to reach a dry density of 1.72 $Mg.m^{-3}$ as a reference state.

Figure 1 shows the variation of the water content with the suction for the compacted soil at its reference state. The van Genuchten equation (van Genuchten 1980) is used to model the Soil Water Retention Curve (SWRC):

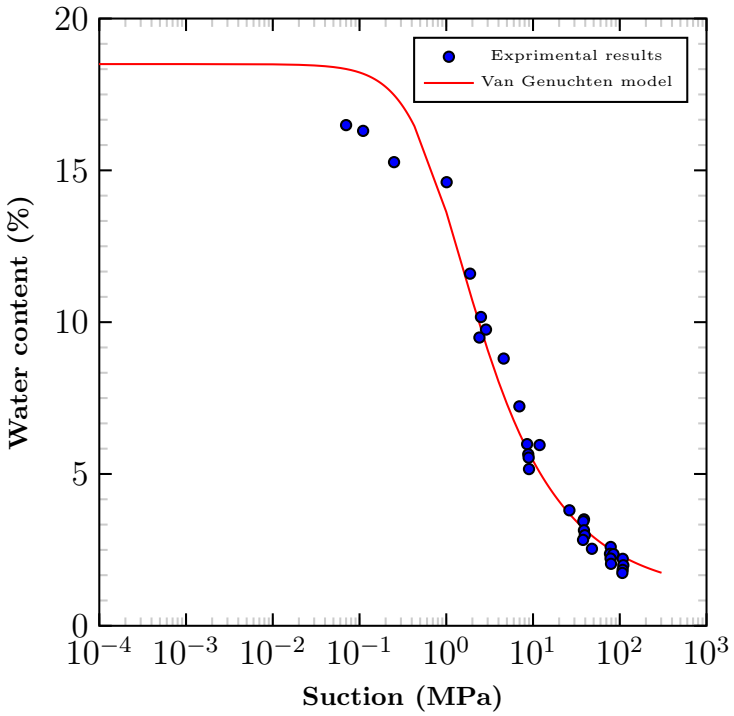

Figure 1: SWRC of the studied compacted backfill soil at reference compaction state (w=16.3% an ρ_d=1.72 $Mg.m^{-3}$)

$$w = w_r + \frac{w_{sat} - w_r}{(1 + (\alpha s)^n)^m} \tag{1}$$

where w is the soil water content at the suction s; w_{sat} and w_r are the saturated water content and the residual water content; α is a parameter related to the air entry suction; m and n are the model constant parameters with $m = 1 - 1/n$. Table 1 summarizes the main parameters of the SWRC used for the studied soil.

Table 1: Hydrothermal properties of the studied soil.

Application	$K(m.s^{-1})$	$l(-)$	$\alpha(m^{-1})$	$n(-)$	$w_r(-)$	$x_s(-)\%$	$\rho_s(Mg.m^{-3})$
Compacted backfill soil	1.10^{-9}	0.5	0.0134	1.52	0.01	0.62	2.60

Figure 2 shows the variation of the hydraulic conductivity of the studied material with

suction. The hydraulic conductivity was measured in saturated conditions with triaxial device and in the unsaturated state with the Wind method (Wind 1966). A combined equation of van Genuchten (1980) and Mualem (1976) is used to calculate hydraulic conductivity with suction:

$$k = K(S_e)^l(1 - (1 - S_e^{1/m})^m)^2 \tag{2}$$

$$S_e = \frac{w - w_r}{w_{sat} - w_r} \tag{3}$$

where K is the saturated hydraulic conductivity ($m.s^{-1}$), S_e is the relative saturation of the soil and l is the pore connectivity parameter. These fitted parameters of Mualem-van Genuchten equation are also summarized in Table 1.

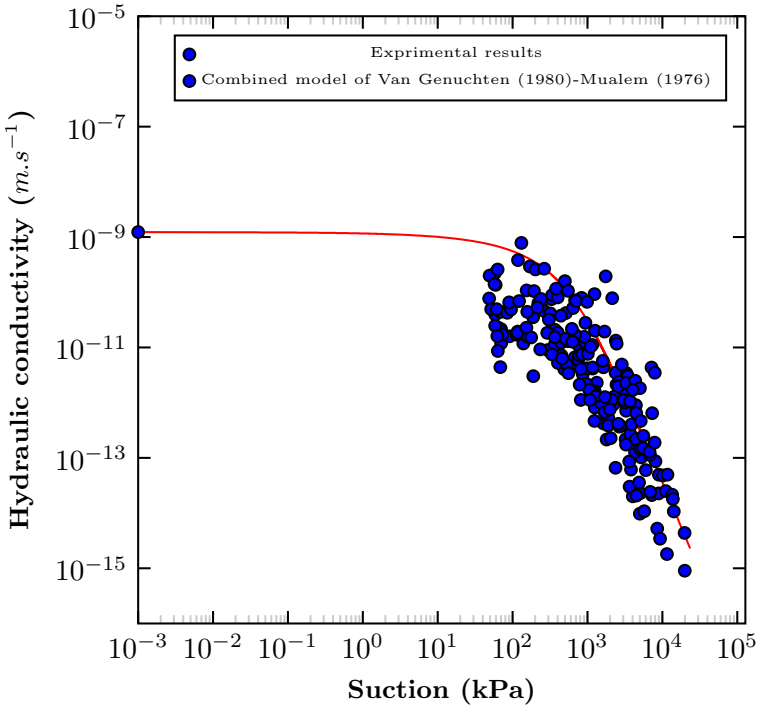

Figure 2: Hydraulic conductivity of the studied backfill soil.

The thermal properties were defined for the reference compaction state of the studied material. The thermal conductivity and volumetric heat capacity were measured by KD2 Pro method (Devices et al. 2016). These values are 2.46 $W.m^{-1}.K^{-1}$ and 3.25.10^6 $J.m^{-3}.K^{-1}$ respectively.

The approach proposed by Nowamooz et al. (2015) and Nikoosokhan et al. (2015) is used to model the soil thermal conductivity:

$$k_s = (0.443x_s + 0.081\gamma_d)\frac{(4.4x_s + 0.4)S_r}{1 + (4.4x_s - 0.6)S_r} + 0.087x_s + 0.019\gamma_d \quad (4)$$

where x_s, γ_d, and S_r are the soil sand content, dry unit weight ($kN.m^{-3}$) and degree of saturation, respectively.

The approach proposed by Tang and Nowamooz (2018a) and Tang and Nowamooz (2018b) is also used to calculate the soil volumetric heat capacity:

$$C_{v-s} = (4.18 - 0.095\gamma_d - 0.3x_s)S_r + 0.09\gamma_d - 0.2x_s \quad (5)$$

3 General conditions of the numerical simulations

General geotechnical, meteorological, hydrothermal and system conditions are given in this section.

3.1 Geotechnical conditions

The studied geometry has a length of 30 m, a width of 12 m and a height of 20 m. This deep geometry is selected to have no hydrothermal impact of the seasonal metrological condition on the bottom boundary. A slinky-type HGHE with 0.03 m of inner diameter and 0.036 m of outer diameter is installed 1 m below surface, covered with the backfill soil compacted at dry densities of 1.72 $Mg.m^{-3}$.

We considered that the HGHE system and its backfill are installed in Alsace region in France in June. The local natural soil surrounding the HGHE till 1 m of depth (installation depth) is completely replaced by the backfill soil (Figure 3). The local soil is mainly constituted of sandy loam and its hydrothermal properties are listed in Table 2.

Table 2: Hydrothermal properties of the subsurface soils.

Application	$K(m.s^{-1})$	$l(-)$	$\alpha(m^{-1})$	n(-)	$w_s(-)$	$w_r(-)$	$x_s(-)$	$\rho_s(Mg.m^{-3})$	$\rho_d(Mg.m^{-3})$
Sandy loam	$1.78.10^{-5}$	0.5	2.60	1.52	0.39	0.02	0.80	2.62	1.60

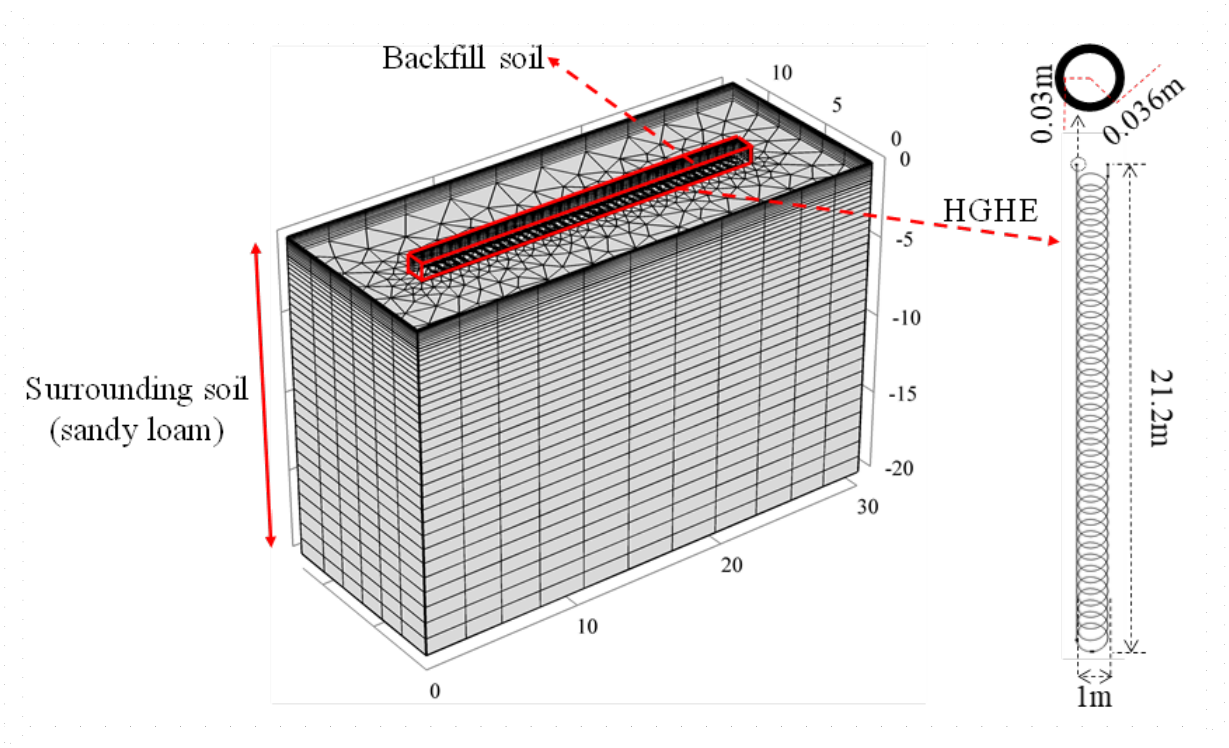

Figure 3: Geometry and its mesh for the numerical simulations.

A swept mesh is deployed to obtain reasonable computation time. It should be noted that the generated meshes are denser in the shallow depths since the shallow ground is more sensitive to hydrothermal fluctuation on the land surface. In addition, the meshes around the HGHE are also denser due to the steep temperature and suction gradients (Choi and Ooka 2016). The geometry and its mesh are shown in Figure 3.

3.2 Boundary and meteorological conditions

The temperature gradient at the bottom boundary is set 0.142 $K.m^{-1}$ (Baillieux et al. 2013), and the extra water from the precipitation is drained at the bottom boundary. The groundwater level is set constant at the depth of 7.5 m in the whole year. No hydrothermal flow is imposed on the lateral boundaries.

The meteorological condition corresponds to the local condition with the installation time in June (Tang and Nowamooz 2018b; Tang and Nowamooz 2019). The parameters for the soil surface energy balance are reported in Table 5 in Appendix. Figure 4a and

Figure 4b present the ambient temperatures and the shortwave radiation for one year represented by a simplified sinusoidal curve.

At the site, there is no obvious seasonal fluctuation of cloud cover, wind speed, precipitation and air humidity with time. Therefore, an average cloud cover of 0.41, an average wind speed of 2 $m.s^{-1}$, an average monthly precipitation of 55.7 mm, and an average air humidity of 83% are applied in the numerical simulation model to capture the main meteorological condition of the local site.

For the surface water balance, 20% of precipitation run off, and the other 80% participate into evapotranspiration or infiltration.

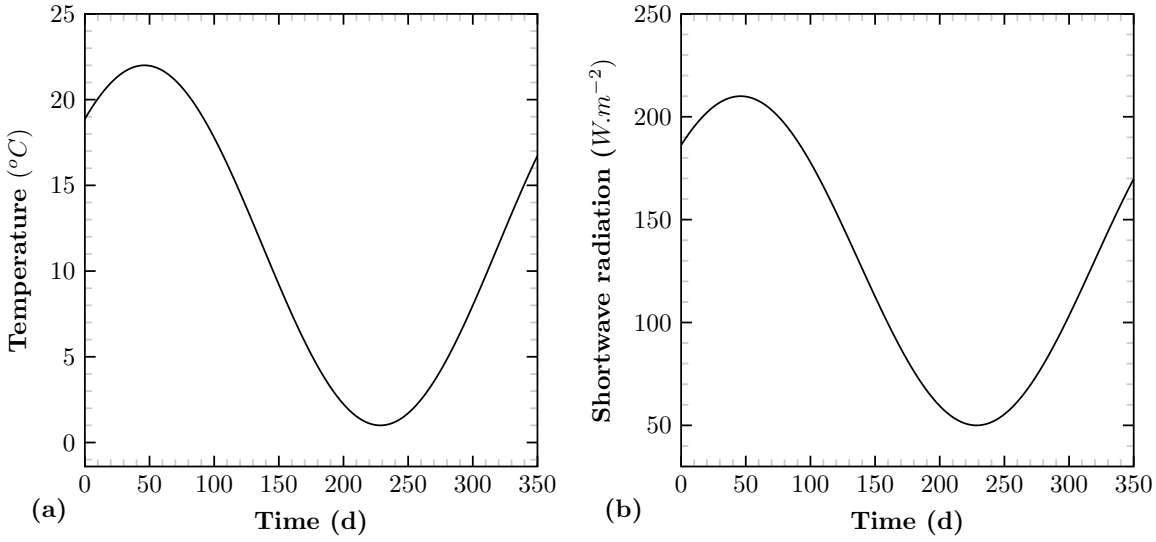

Figure 4: Simplified local meteorological condition: (a) ambient temperature fluctuation for one year and (b) shortwave radiation fluctuation for one year.

3.3 Initial hydrothermal conditions

An equilibrium method is used to obtain the initial hydrothermal profiles at its installation time in the end of summer. Figure 5 shows the suction and temperature profiles at this time.

3.4 Pipe and its carrying fluid

The pipe is a High-Density Polyethylene Pipe (HDPE) with the thermal conductivity of 0.4 $W.m^{-1}.K^{-1}$. Propylene Glycol (PG) with a volume concentration of 25% is selected as

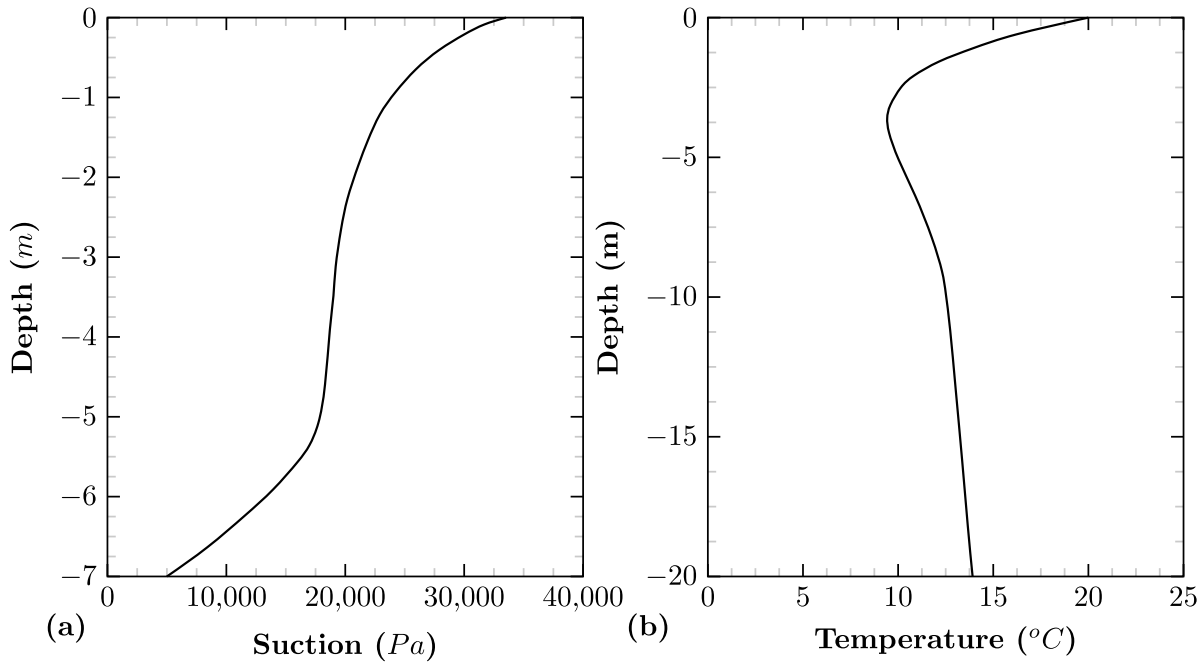

Figure 5: Initial hydrothermal profiles: (a) suction profile and (b) temperature profile.

the carrying fluid. It has a dynamic viscosity of 0.0055 $Pa.s$, a density of 1026 $kg.m^{-3}$, a thermal conductivity of 0.45 $W.m^{-1}.K^{-1}$ and a specific heat capacity of 3974 $J.kg^{-1}.K^{-1}$ (Casasso and Sethi 2014). The carrying fluid velocity is 0.5 $m.s^{-1}$ during the operation period.

4 Validation of the proposed numerical framework

The atmosphere-soil and soil-HGHE interactions are separately evaluated to validate the atmosphere-soil-HGHE interaction in our numerical simulation framework. A brief verification is shown in this section, the detailed verification for the numerical simulation model is provided in Tang and Nowamooz (2020).

The atmosphere-soil interaction was evaluated by using a local instrumented temperature probe (Lin et al. 2020). Figure 6 shows the comparison of the numerical prediction for a duration of 3 years from July 2014 to July 2017. The comparison shows that the numerical framework is capable to predict the soil temperature with the Root-Mean-Square Error (RMSE) value of 1.6 ^oC, proving that atmosphere-soil interaction in the numerical simulation predict reasonably well the in-situ measurement.

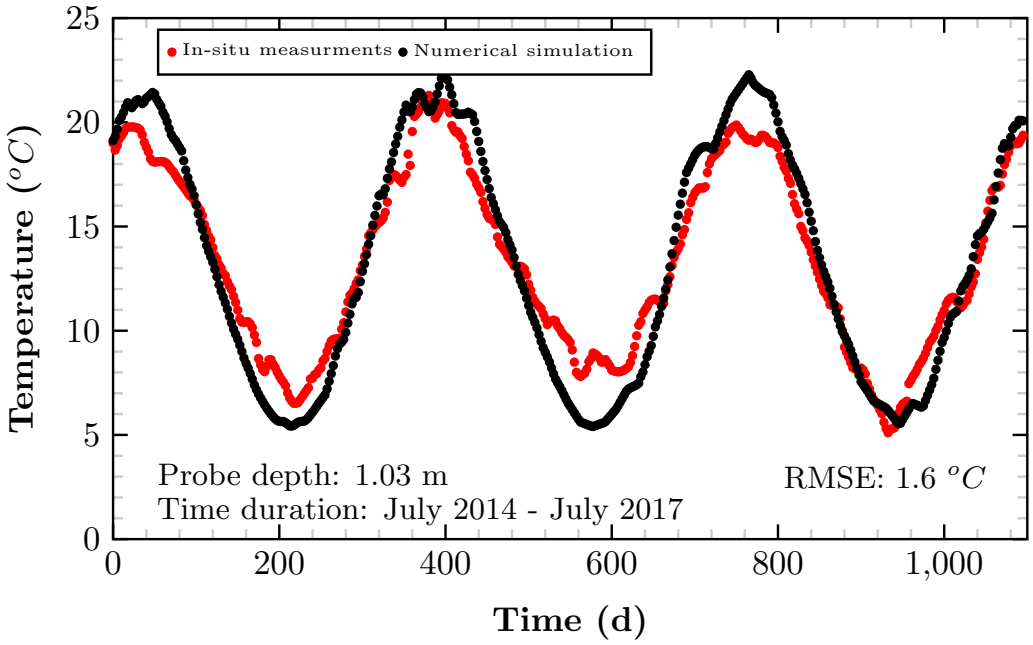

Figure 6: mparison between the numerical predictions and the in-situ measurements for 3 years from July 2014 to July 2017 (Lin et al. 2020).

The soil-HGHE interaction was evaluated by an indoor experiment performed by Yoon et al. (2015). Figure 7 shows the comparison between the experiment and prediction for the carrying fluid outlet temperatures. A good correspondence between the experiment and prediction proves that the proposed numerical model considers appropriately the soil-HGHE interaction in its framework.

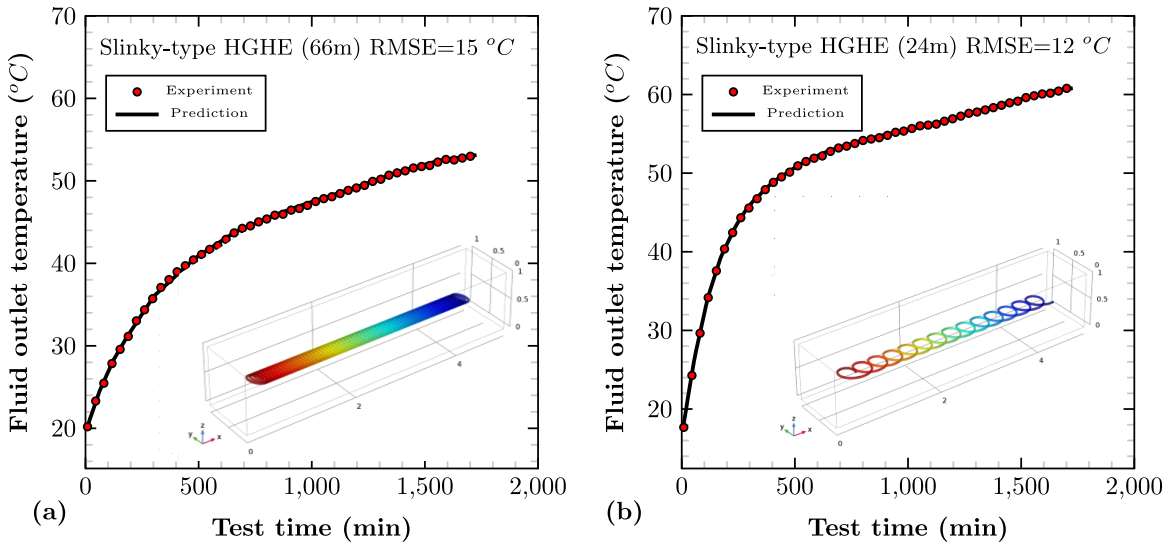

Figure 7: The comparison between the experiment and prediction for the carrying fluid outlet temperatures: (a) slinky-type HGHE with a total pipe length of 24 m and (b) slinky-type HGHE with a total pipe length of 66 m.

5 Comparison of performances of HGHE installed in the local and compacted backfill soils

The numerical simulations consider the atmosphere-soil-HGHE interaction in its framework. Tang and Nowamooz (2020) proposed a numerical framework for the atmosphere-soil-HGHE interaction. To avoid the repetition of the numerical framework, some principal equations of this numerical framework are reported in Appendix (Figure 16 and Table 4). To show the suitable hydro-thermal efficiency of backfill material, the performance of installed HGHE is also compared to the same system installed in the local sandy loam (Tang and Nowamooz 2018a). The system has been designed to extract the shallow geothermal energy. Therefore, a heating scenario is considered according to the local climate condition presented in section 3.2. The HGHE works from the end of Autumn season up to the end of Winter season (Figure 4a). During working times, a fluid with the inlet temperature of 1 ^oC circulated through the HGHE to exploit the geothermal energy. The inlet temperature of 1 ^oC is conventionally selected because of the thermal performance of the HGHE system. The HGHE is installed in compacted backfill and local soil in which their hydrothermal properties were presented in Tables 1 and 2 respectively.

During the service time of the HGHE, the Total Extracted Energy (TEE) can be obtained with time (t) by the following equation:

$$TEE = \int A\rho_f u_f C_{p-f}(T_{out} - T_{in})dt \tag{6}$$

where T_{in} is the fluid inlet temperature (^oC), T_{out} is the fluid outlet temperature (^oC), A is the pipe inner cross-sectional area (m^2), ρ_f is the fluid density ($kg.m^{-3}$), C_{p-f} is the fluid specific heat capacity ($J.kg^{-1}.K^{-1}$) and u_f is the fluid flowing velocity ($m.s^{-1}$).

The mesh number and time step verifications for the model are additionally brought out. Four mesh numbers indicating 38826, 53654, 78383 and 117866 are taken into account. Five time steps representing 1.5, 1.25, 1, 0.75 and 0.5 days are compared to choose the optimal one. The results show that there is a decrease accuracy of the TEE with the decrease of mesh number and increase of time step. The results show that the accuracy

of the numerical simulation model could be satisfied with the mesh number of 78383 and the time step of 1 day (Figure 8).

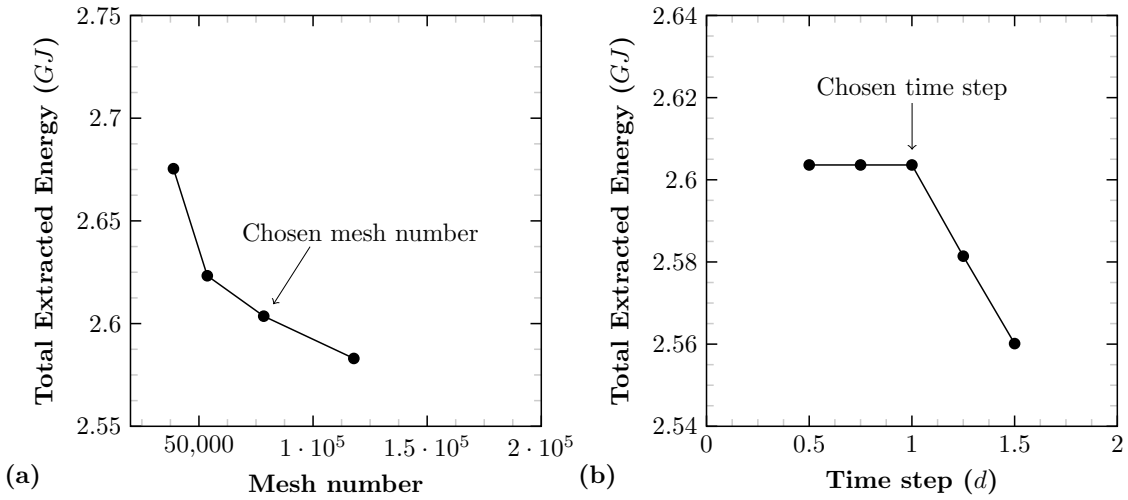

Figure 8: (a) mesh number and (b) time step verifications for the numerical simulation model.

Figure 9a shows the TEE of the HGHE during its annual working period for the local and compacted backfill soils. It shows that the installed HGHE can extract 2.95 GJ and 2.49 GJ of energy after 1 year respectively for compacted backfill and local soil. It shows that the compacted backfill soil increases 18.5% the system performance which is mainly due to its higher initial thermal conductivity (Figure 9b).

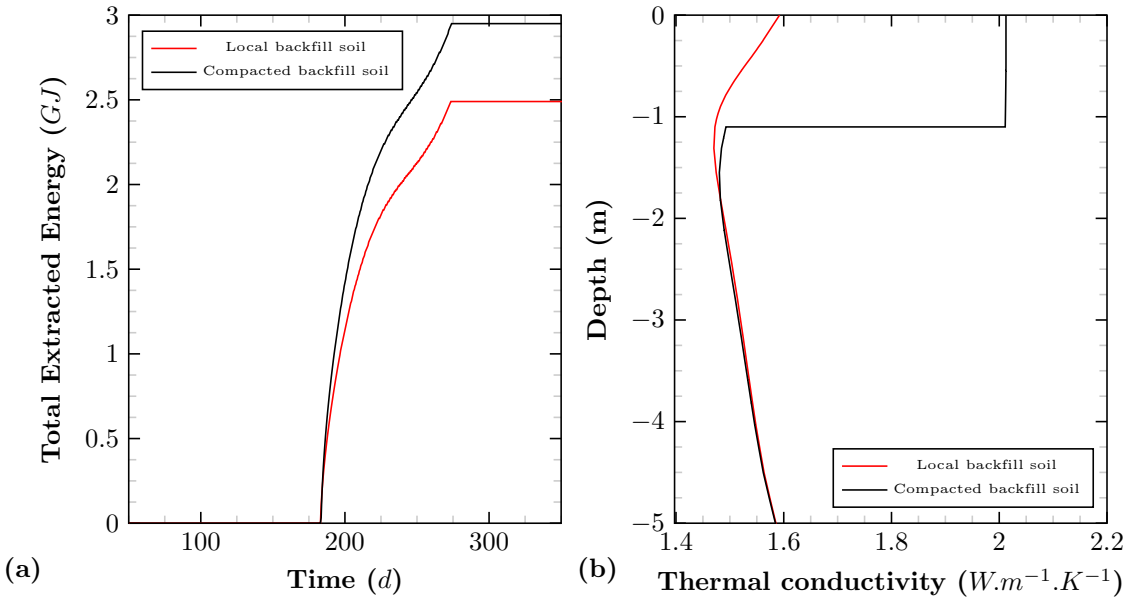

Figure 9: (a) the extracted energy with time during the service period of the HGHE for compacted backfill and local soils installed at the depth of 1 m, (b) the initial thermal conductivity profiles for the local and compacted backfill soils.

The whole simulation results show that the hydrothermal characteristics of backfill material are highly better than the local soil. It is recommended to use this backfill material in the HGHE system however it adds some costs for its excavation and transportation. Therefore, the geotechnical investigations of the local materials are crucial to conclude if they should be substituted by a backfill material.

6 Heat storage effect on the performance of HGHE installed in the compacted backfill soil

In this section, the effect of thermal energy storage during summer on the HGHE performance installed in different depths compacted backfill soil is investigated. The results are compared to the original system with no heat storage (called Nsto scenario in this section).

6.1 Energy storage scenarios and installation depths

The context of thermal energy storage increases the performance of the HGHE by increasing the temperature of ground. Therefore, during summer, a fluid with higher temperature than the ground can circulate through the HGHE to exchange the temperature with surrounding soil. The stored heat is expected to be released during winter. The stored energy during summer season is extracted by a circulating fluid with a temperature of 1^oC in the HGHE during winter. The system stops working at the end of Winter.

To store thermal energy in soil during summer season and use it in winter, two different scenarios are investigated in this study:

a) First scenario (StoA)

A reservoir of carrying fluid is exposed to exterior temperature and then the carrying fluid circulates in HGHE during summer. Therefore, the inlet temperature in 3 months of summer is the ambient temperature (scenario StoA) as presented in Figure 10 (temperatures of 0 to 92 days). This system is in relaxation in Autumn (from 92nd to 183rd day), therefore no fluid flow will be circulated through the system. When Winter comes

(from 183rd to 274th day), a fluid flow with inlet temperature of 1^oC will be circulated. Again the system is in relaxation in Spring (from 274rd to 365th day) (Table 3).

b) Second scenario(Sto50)

Solar panels absorb the solar energy and the energy can be used to heat the subsurface soil in summer while a fluid with a constant inlet temperature is circulating in the HGHE. Therefore, the inlet temperature in 3 months of summer is a constant temperature of 50 ^oC (Sto50) as presented in Figure 10. The system works the same way as the ambient temperature storage scenario except that the inlet temperature is 50 ^oC in Summer season (Table 3).

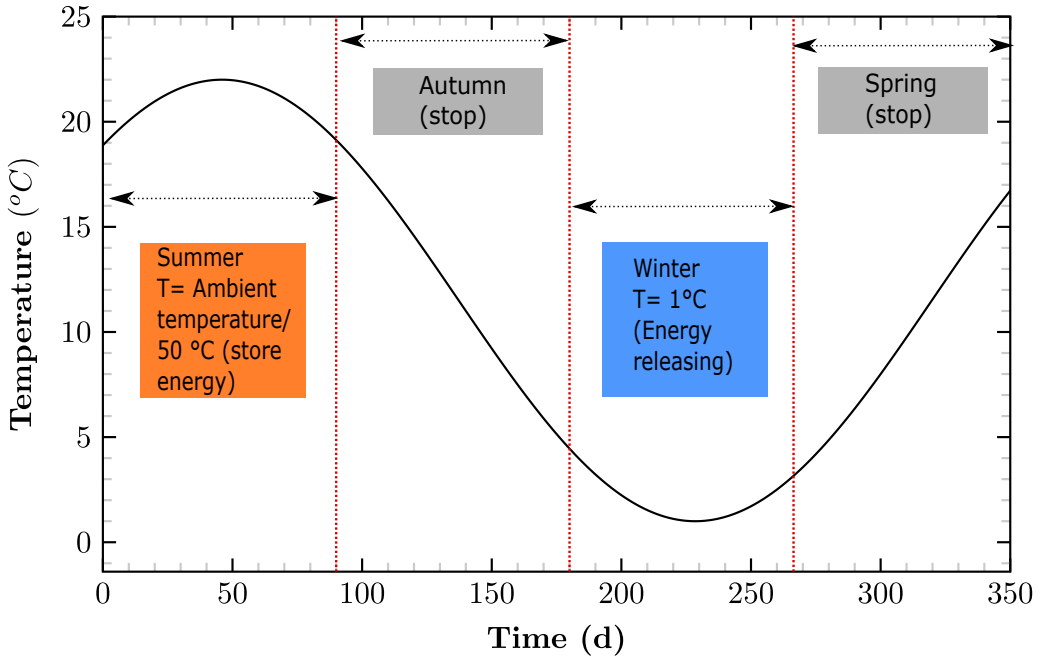

Figure 10: Operation mode for the HGHE over one year.

Table 3: Imposed temperature of inlet fluid for StoA and Sto50.

Scenario	Summer (0 to 92^{th} days)	Autumn (92^{nd} to 183^{rd} day)	Winter (183^{rd} to 274^{th} day)	Spring (274^{rd} to 365^{th} day)
StoA	Ambient temperature Figure 4a	Relaxation	1 ^oC	Relaxation
Sto50	50 ^oC	Relaxation	1 ^oC	Relaxation

Due to the interaction with ground surface, the stored energy during relaxation seasons is dissipated into the atmosphere. If the HGHE is installed close to the land surface, a

higher amount of stored energy can be dissipated. Therefore, three depths of 1, 1.5 and 2 m beneath land surface are investigated for both scenarios to study the influence of installation depth on the HGHE performance.

6.2 Simulation results

a) Scenario 1 (StoA) compared to scenario with no heat storage (Nsto)

Figure 11 shows the pipe outlet temperature with time at the installation depths of 1, 1.5 and 2 m for the first scenario (StoA) compared to the outlet temperatures of the original HGHE with no heat storage (Nsto) presented in section 5. The figure shows the fluid outlet temperature decreases abruptly with the working of the HGHE. Afterwards, the fluid temperature generally decreases and starts to increase with warmer climate. In addition, the figure shows that outlet temperature increases slightly by depth.

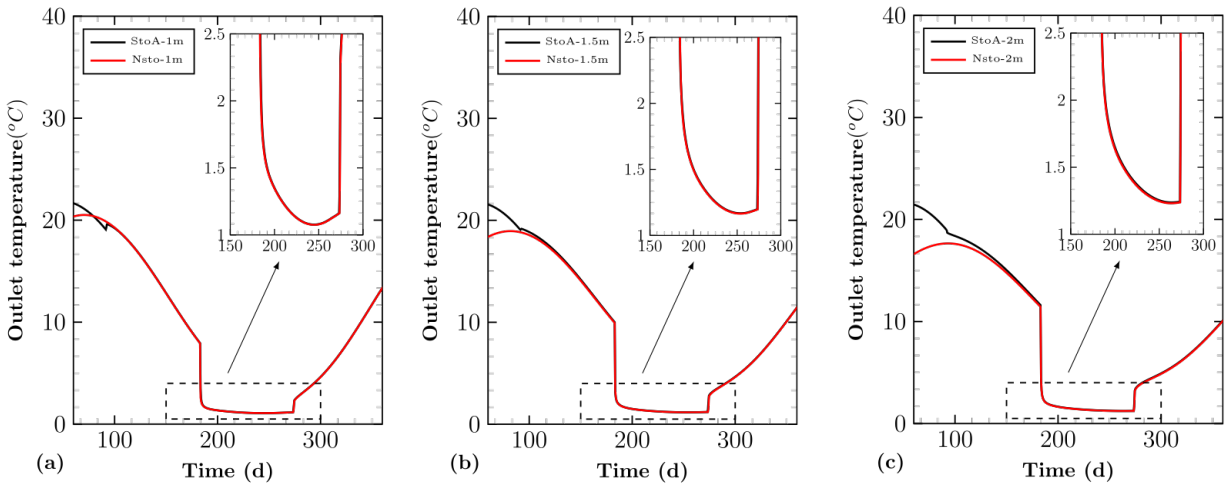

Figure 11: Outlet temperature comparison of the storage scenario (ambient temperature) and the non-storage scenario for three installation depths (a) 1m, (b) 1.5m and (c) 2m.

b) Scenario 2 (Sto50) compared to scenario with no heat storage (Nsto)

Figure 12 shows the outlet temperature for the second storage scenario (Sto50) at three installation depths compared to the outlet temperatures of the original HGHE with no heat storage (Nsto) presented in section 5. The figure shows that the ground temperature is obviously improved in summer, and the deeper the installation depth, the larger difference between the outlet temperatures of the scenario considering and non-considering the energy storage in summer.

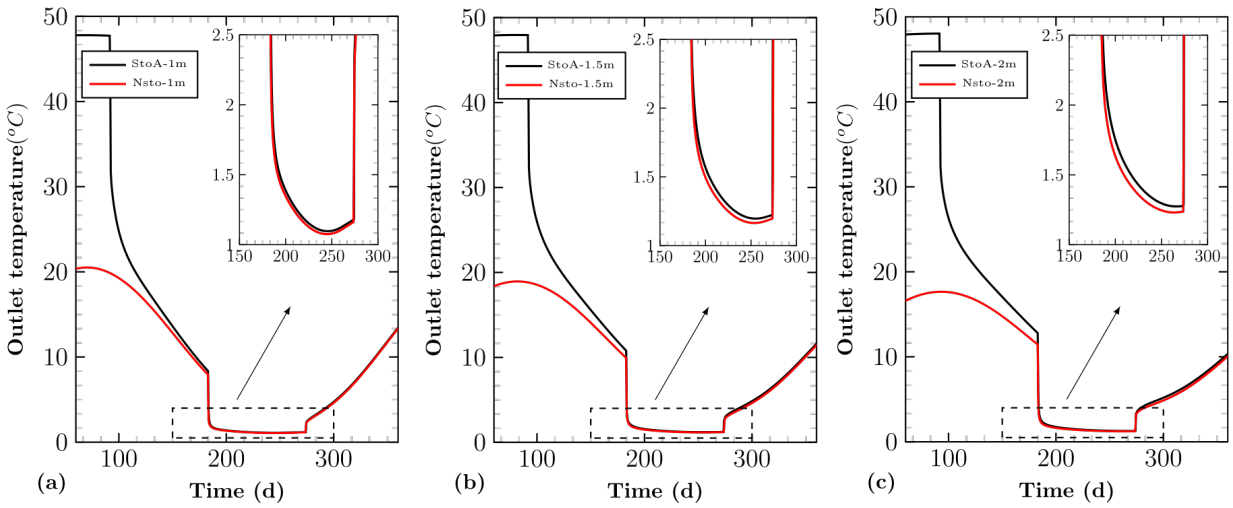

Figure 12: Outlet temperature comparison of the storage scenario (50 ^oC of inlet temperature during summer) and the non-storage scenario for three installation depths (a) 1m, (b) 1.5m and (c) 2m.

As presented in section 5, the backfill soil is recommended for the good performance of the HGHE system. In this section, the different energy storage scenarios and the installation depths are also investigated. To optimize the system performance, it is necessary to compare these different configurations together.

7 Comparison of the two energy storage scenarios

The surrounding temperatures of the HGHE installed at the depth of 2 m in the end of Summer, Autumn and Winter are shown in Figure 13. The figure shows that the soil temperature has been clearly improved in the scenario with 50 ^oC of fluid inlet temperature in Summer (Sto50), while the surrounding temperature improves negligibly with the ambient temperature storage scenario (StoA). Specifically, soil temperature has been improved 27 ^oC and 3 ^oC respectively at the depth of 2 m at the end of Summer and Autumn with the energy storage scenario (Sto50).

By using equation 6, the corresponding extracted energies can be exploited with time for both scenarios as presented in Figure 14. The results show that the heat storage can improve the TEE and the improvement increases with depth in both scenarios. This increase is more evident for the scenario Sto50. Specifically, for the installation depth of 1 m, this increase is 0.34 GJ (13.7%) compared to 0.0 GJ (0.0%). When the installation

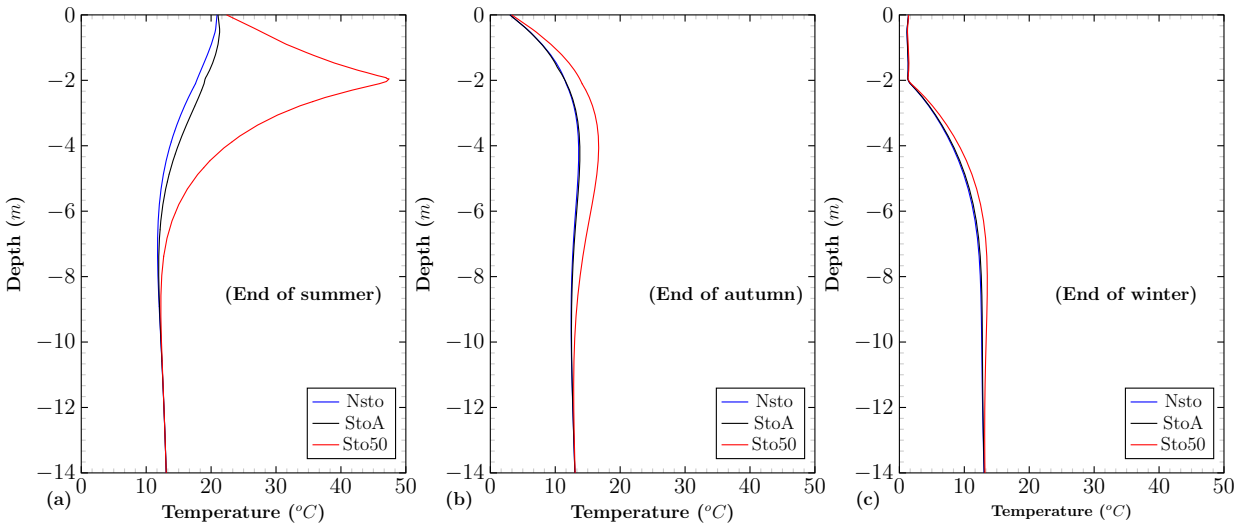

Figure 13: Temperature profiles at the end of (a) Summer , (b) Autumn and (c) Winter.

depth increases from 1 to 2 m, the final improvement of the TEE increases from 0.0 GJ to 0.12 GJ (0.0 to 4.8%) for the first scenario StoA (Figure 14a) while it increases form 0.34 GJ to 1.03 GJ (13.7 to 41.4%) for the second scenario (Sto50).

Figure 15 compares the annual TEE values of the aforementioned heat storage scenarios (StoA and Sto50) with the TEE values of the original scenario without heat storage (Nsto). The figure shows that the HGHE can be highly improved by adopting an inlet fluid temperature of 50^oC in summer while the ambient inlet temperature produces less amelioration in the HGHE performance.

The simulations show clearly that a higher installation of the backfill material accompanied with the Sto50 scenario produce the best performance for the HGHE. However , some additional costs are to be considered for a deeper installation. Therefore, it is recommended to add a cost overview for the different installation depths of the backfill material compared to local materials to find an optimized depth for the HGHE system.

8 Conclusions

This work brings some insights into the selection of the backfill soil on the performance of a HGHE. Moreover, two energy storage scenarios and three installation depths have been adopted to investigate the HGHE performance. A well-known compacted backfill

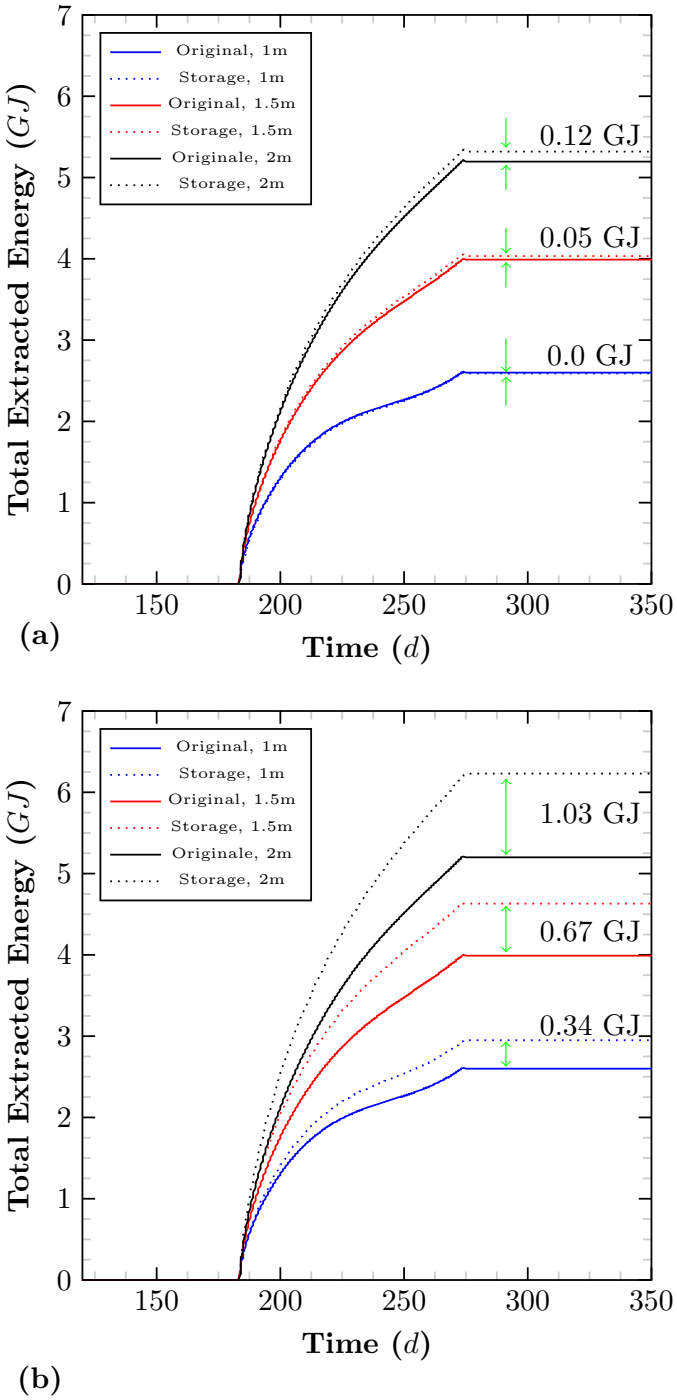

Figure 14: Total extracted energy with time of (a) first scenario (StoA) and (b) second scenario (Sto50) compared to the original HGHE system (Nsto).

soil was used to improve the performance of a HGHE system installed in the east of France. The hydrothermal properties of the backfill soil were first injected in a numerical framework considering the atmosphere-soil-HGHE interaction. The simulations results showed that the compacted backfill material provided an increase 18.5% in the HGHE

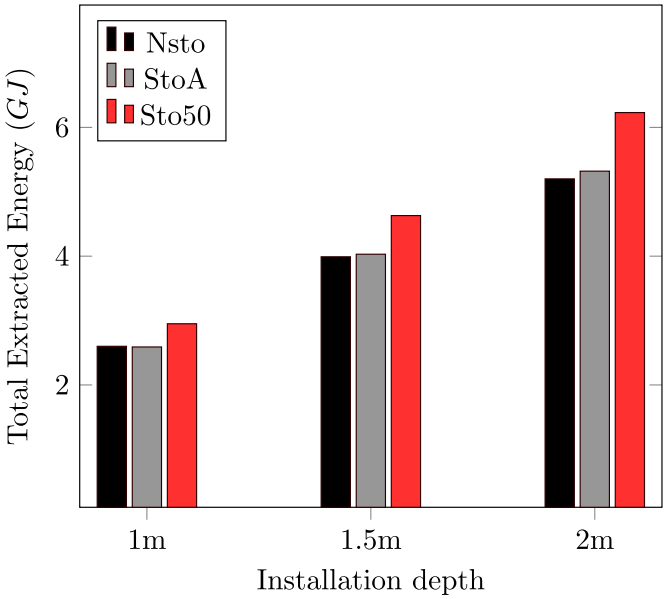

Figure 15: Comparison between the heat storage scenarios (StoA and Sto50) with non-storage scenario (Nsto) at three different installation depths.

performance compared to the existing local soil. To improve the HGHE performance, two heat storage scenarios at three different installation depths were studied. The results showed that an inlet fluid temperature of 50 ^oC in summer increased highly the system performance (13.7 to 41.4%) while the improvement was less significant (0 to 4.8%) for the ambient inlet temperature. A deeper installation depth increased the total extracted energy (TEE) but increases the installation costs. This study has focused only on one metrological region and further analysis are still necessary to combine the meteorological conditions with the selection of the backfill material used in the HGHE systems.

A Appendix: Governing Equations

Figure 16 shows a schematic diagram of the concerning phenomenon in HGHE engineering. The necessary governing equations considering the atmosphere-soil-HGHE interaction are constituted of 4 parts: a) the soil surface energy balance; b) the soil surface water balance; c) the hydrothermal transfer in subsurface soil and d) the heat transfer in pipe. All these equations were already published in Tang and Nowamooz (2020). A summary of these equations is presented in Table 4.

In Table 4, R_n is the net radiation heat flux ($W.m^{-2}$), H is the sensible heat flux

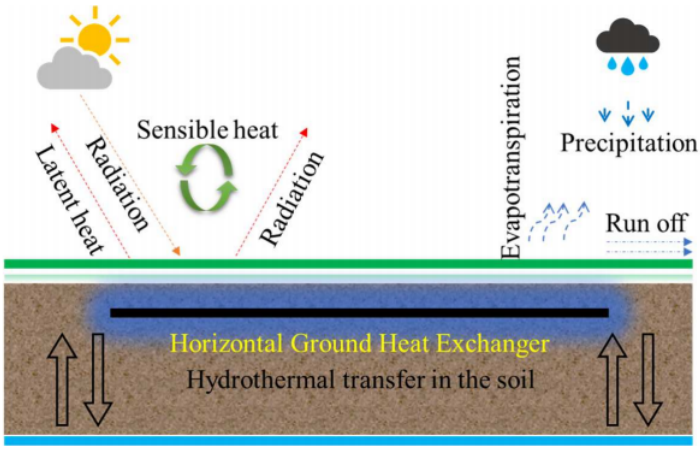

Figure 16: Comparison between the heat storage scenarios (StoA and Sto50) with non-storage scenario (Nsto) at three different installation depths.

$(W.m^{-2})$, LE is the latent heat flux $(W.m^{-2})$, G is the ground heat flux $(W.m^{-2})$, a_l is the surface albedo, R_s is the shortwave radiation $(W.m^{-2})$, R_a is the incoming longwave radiation $(W.m^{-2})$, $\varepsilon\sigma T_s^4$ is the outcoming longwave radiation $(W.m^{-2})$, ε is the soil surface emissivity, σ is Stephan-Boltzman constant $(W.m^{-2}.k^{-4})$, T_s is the soil temperature (K), ρ_a is the air density $(kg.m^{-3})$, C_{P-a} is the air specific heat capacity $(J.kg^{-1}.K^{-1})$, r_a is the aerodynamic resistance to heat transfer $(s.m^{-1})$, P is the rainfall rate $(mm.s^{-1})$, E_p is the evaporation potential $(mm.s^{-1})$, LAI is the leaf area index, h_c is the displacement height is linear o the vegetation height (m), W_r is the water run off, E is the actual evaporation, W_i is the infiltration, ρ_w is the water density $(kg.m^{-3})$, Ψ is the specific moisture capacity (m^{-1}), H_p is the suction head (m), t is the time (s), K is the saturated hydraulic conductivity $(m.s^{-1})$, k_r is the relative hydraulic conductivity, D is the elevation head (m), H_k is the kinetic head (m), ρ_s is the soil density $(kg.m^{-3})$, C_{p-s} is the soil heat capacity $(J.kg^{-1}.K^{-1})$, C_{p-w} is the water specific heat capacity $(J.kg^{-1}.K^{-1})$, u_w is the water velocity in soil $(m.s^{-1})$, Q_s is the soil heat source $(W.m^{-3})$, A is the pipe inner cross-sectional area (m^2), ρ_f is the fluid density $(kg.m^{-3})$, C_{p-f} is the fluid specific heat capacity $(J.kg^{-1}.K^{-1})$, T_f is the fluid temperature (^oC), u_f is the fluid flowing velocity $(m.s^{-1})$, k_f is the fluid thermal conductivity $(W.m^{-1}.K^{-1})$, f_D is the Darcy friction factor, d_h is the hydraulic diameter (m) and Q_{wall} is the energy from the surrounding media $(W.m^{-1})$, h_{int} is the film heat transfer coefficient $(W.m^{-2}.K^{-1})$, Z is the pipe inner

perimeter (m) and T_{i-p} is the inner pipe temperature (^oC).

Table 4: Principal equations of atmosphere-soil-HGHE interaction.

Type of interaction	Principal equation
soil surface energy balance (Turc 1954; Pike 1964; Monteith 1965; Allen et al. 1989; Gerrits et al. 2009; Chalhoub et al. 2017; Chen and Buchberger 2018)	$R_n + H - LE - G = 0$ $R_n = (1 - a_l)R_s + (R_a - \varepsilon\sigma T_s^4)$ $H = \rho_a C_{P-a}(T_a - T_s)/r_a$ $E = P.[1 + (E_p/P)^{-2}]^{1/2}$ LAI=24.h_c for clipped grass or LAI=5.5+1.5 ln h_c for other crops
Soil surface water balance (Dietrich et al. 2016)	$P = W_r + E + W_i$
Richard equation for hydraulic transfer is soil (Wind 1966; Mualem 1976; van Genuchten 1980)	$\rho_w.\Psi.\frac{dH_P}{dt} + [-K.k_r.\nabla.\rho_w.(H_P + D + H_k)] = 0$
Hydrothermal transfer in subsurface soil (Nowamooz et al. 2015; Nikoosokhan et al. 2015; Tang and Nowamooz 2018a; Tang and Nowamooz 2018b)	$\rho_s C_{p-s}\frac{dT_s}{dt} = \nabla.(k_s\nabla T_s) + \nabla.(\rho_s C_{p-s} u_w T_s) + Q_s$
Heat transfer in pipe	$A\rho_f C_{p-f}\frac{dT_f}{dt} + A\rho_f C_{p-f} u_f.\nabla T_f = \nabla.Ak_f\nabla.T_f + f_D\frac{\rho_f A}{2d_h}\lvert u_f\rvert u_f^2 + Q_{wall}$ $Q_{wall} = h_{int}.Z.(T_{i-p} - T_f)$

Table 5: Parameters for the soil surface energy balance.

Parameter	Description	Value	Unit
a_l	Albedo	0.25	-
ε	Soil emissivity	0.97	-
σ	Stephan-Boltzman constant	5.67×10^{-8}	$W.m^{-2}.K^{-4}$
ρ_a	Air density	1.25	$kg.m^{-3}$
C_{p-a}	Air specific heat capacity	1.00×10^3	$J.kg^{-1}.K^{-1}$
z_m	Height to collect the meteorological data	2.00	m
h_c	Grass height	0.06	m
k	von Karman constant	0.41	-
L	Latent heat of vaporization	2.26	$J.kg^{-1}$
p_{at}	Atmospheric pressure	102000	Pa
r_{mw}	Molecular weight of water vapor to dry air	0.62	-
r_1	Stomatal resistance of a single leaf	100	$s.m^{-1}$

Nomenclature

A	U-pipe cross-sectional area, m^2
a_l	surface albedo
C_p	specific heat capacity, $J.kg^{-1}.K^{-1}$
C_v	volumetric heat capacity, $J.m^{-3}.K^{-1}$
D	elevation head, m
E_p	evaporation potential, $kg.m^{-2}.s^{-1}$ or $mm.s^{-1}$
d_h	inner diameter of the U-pipe, m
f_D	Darcy friction factor
G	total heat flux through land surface, $W.m^{-2}$
h_c	vegetation height, m
h_{int}	heat transfer coefficient, $W.m^{-2}.K^{-1}$
H	sensible heat flux, $W.m^{-2}$
H_k	kinetic head, m
H_p	water potential or suction head, m
k	thermal conductivity, $W.m^{-1}.K^{-1}$
k_r	relative hydraulic conductivity
K	hydraulic conductivity, $m.s^{-1}$
l	pore connectivity parameter
L	latent heat of vaporization for water, $J.kg^{-1}$

LAI	leaf area index
n	independent parameter
P	rainfall rate, $mm.s^{-1}$
P_{at}	atmospheric pressure, Pa
Q_s	soil heat source, $W.m^{-3}$
Q_{wall}	heat from the surrounding, $W.m^{-1}$
r_1	stomatal resistance of a single leaf, $s.m^{-1}$
r_a	aerodynamic resistance to heat transfer, $s.m^{-1}$
r_c	crop canopy resistance, $s.m^{-1}$
r_{mw}	molecular weight of water vapor to dry air
R_n	net radiation, $W.m^{-2}$
R_s	shortwave radiation, $W.m^{-2}$
S_e	relative saturation of soil
S_r	saturation of soil
t	time, s
T	temperature, ^oC or K
T_{in}	inlet temperature, ^oC
T_{out}	outlet temperature, ^oC
T_s	land surface temperature, K
u	velocity, $m.s^{-1}$

w	water content
W_i	infiltration, $mm.s^{-1}$
W_r	water run off, $mm.s^{-1}$
x_s	gravimetric sand content
Z	U-pipe inner perimeter, m
z_m	height for measuring meteorological conditions, m

Greek symbols

α	independent parameter, m^{-1}
γ_d	soil dry unit weights, $kN.m^{-3}$
γ_s	soil specific unit weights, $kN.m^{-3}$
ε	soil surface emissivity
k	von Karman constant
ρ	density, $kg.m^{-3}$
σ	Stephan-Boltzman constant, $W.m^{-2}.K^{-4}$

Subscripts

a	air
f	carrying fluid
i-p	inner pipe wall
r	residual
s	soil
sat	saturated

w water

References

Abu-Hamdeh, N. H. and Reeder, R. C., 2000. Soil thermal conductivity effects of density, moisture, salt concentration, and organic matter, *Soil science society of America Journal* **64**(4): 1285–1290.

Adamovsky, D., Neuberger, P. and Adamovsky, R., 2015. Changes in energy and temperature in the ground mass with horizontal heat exchangers—the energy source for heat pumps, *Energy and Buildings* **92**: 107–115.

Allen, R. G., Jensen, M. E., Wright, J. L. and Burman, R. D., 1989. Operational estimates of reference evapotranspiration, *Agronomy journal* **81**(4): 650–662.

Asgari, B., Habibi, M. and Hakkaki-Fard, A., 2020. Assessment and comparison of different arrangements of horizontal ground heat exchangers for high energy required applications, *Applied Thermal Engineering* **167**: 114770.

ASTM, E., 2000. Standard practice for classification of soils for engineering purposes (unified soil classification system), *Annual book of ASTM standards* .

Baillieux, P., Schill, E., Edel, J.-B. and Mauri, G., 2013. Localization of temperature anomalies in the upper rhine graben: insights from geophysics and neotectonic activity, *International Geology Review* **55**(14): 1744–1762.

Beier, R. A. and Holloway, W. A., 2015. Changes in the thermal performance of horizontal boreholes with time, *Applied Thermal Engineering* **78**: 1–8.

Boukelia, A., 2016. *Physical and numerical modeling of energy geostructures, PhD thesis.*, PhD thesis, University of lorraine.

Casasso, A. and Sethi, R., 2014. Efficiency of closed loop geothermal heat pumps: a sensitivity analysis, *Renewable Energy* **62**: 737–746.

Chalhoub, M., Bernier, M., Coquet, Y. and Philippe, M., 2017. A simple heat and moisture transfer model to predict ground temperature for shallow ground heat exchangers, *Renewable energy* **103**: 295–307.

Chen, X. and Buchberger, S. G., 2018. Exploring the relationships between warm-season precipitation, potential evaporation, and "apparent" potential evaporation at site scale, *Hydrology and Earth System Sciences* **22**(8): 4535.

Choi, W. and Ooka, R., 2016. Effect of disturbance on thermal response test, part 2: Numerical study of applicability and limitation of infinite line source model for interpretation under disturbance from outdoor environment, *Renewable Energy* **85**: 1090–1105.

Devices, D. et al., 2016. Kd2 pro thermal properties analyzer operator's manual, *Pullman, WA* .

Dietrich, O., Fahle, M. and Seyfarth, M., 2016. Behavior of water balance components at sites with shallow groundwater tables: Possibilities and limitations of their simulation using different ways to control weighable groundwater lysimeters, *Agricultural Water Management* **163**: 75–89.

Elminshawy, N. A., Siddiqui, F. R., Farooq, Q. U. and Addas, M. F., 2017. Experimental investigation on the performance of earth-air pipe heat exchanger for different soil compaction levels, *Applied Thermal Engineering* **124**: 1319–1327.

Florides, G. and Kalogirou, S., 2007. Ground heat exchangers—a review of systems, models and applications, *Renewable energy* **32**(15): 2461–2478.

Gan, G., 2013. Dynamic thermal modelling of horizontal ground-source heat pumps, *International Journal of Low-Carbon Technologies* **8**(2): 95–105.

Gao, Y., Fan, R., Li, H., Liu, R., Lin, X., Guo, H. and Gao, Y., 2016. Thermal performance improvement of a horizontal ground-coupled heat exchanger by rainwater harvest, *Energy and Buildings* **110**: 302–313.

Gerrits, A., Savenije, H., Veling, E. and Pfister, L., 2009. Analytical derivation of the

budyko curve based on rainfall characteristics and a simple evaporation model, *Water Resources Research* **45**(4).

Gonzalez, R. G., Verhoef, A., Vidale, P. L., Main, B., Gan, G. and Wu, Y., 2012. Interactions between the physical soil environment and a horizontal ground coupled heat pump, for a domestic site in the uk, *Renewable energy* **44**: 141–153.

H Abedin, A. and A Rosen, M., 2011. A critical review of thermochemical energy storage systems, *The open renewable energy journal* **4**(1).

Habibi, M. and Hakkaki-Fard, A., 2018. Evaluation and improvement of the thermal performance of different types of horizontal ground heat exchangers based on techno-economic analysis, *Energy Conversion and Management* **171**: 1177–1192.

Hurtado, F., Kaiser, A. and Zamora, B., 2012. Evaluation of the influence of soil thermal inertia on the performance of a solar chimney power plant, *Energy* **47**(1): 213–224.

Jradi, M., Veje, C. and Jørgensen, B., 2017. Performance analysis of a soil-based thermal energy storage system using solar-driven air-source heat pump for danish buildings sector, *Applied Thermal Engineering* **114**: 360–373.

Lahoori, M., Jannot, Y., Rosin-Paumier, S., Boukelia, A. and Masrouri, F., 2020. Measurement of the thermal properties of unsaturated compacted soil by the transfer function estimation method, *Applied Thermal Engineering* **167**: 114795.

Lahoori, M., Rosin-Paumier, S., Stoltz, G. and Jannot, Y., 2020. Thermal conductivity of nonwoven needle-punched geotextiles: effect of stress and moisture, *Geosynthetics International* pp. 1–30.

Lee, C., You, J. and Park, H., 2018. In-situ response test of various borehole depths and heat injection rates at standing column well geothermal heat exchanger systems, *Energy and Buildings* **172**: 201–208.

Li, C., Cleall, P. J., Mao, J. and Muñoz-Criollo, J. J., 2018. Numerical simulation of ground source heat pump systems considering unsaturated soil properties and groundwater flow, *Applied Thermal Engineering* **139**: 307–316.

457 Lin, J., Nowamooz, H., Braymand, S., Wolff, P. and Fond, C., 2020. Impact of soil
458 moisture on the long-term energy performance of an earth-air heat exchanger system,
459 *Renewable Energy* **147**: 2676–2687.

460 Monteith, J. L., 1965. Evaporation and environment, *Symposia of the society for experi-*
461 *mental biology*, Vol. 19, Cambridge University Press (CUP) Cambridge, pp. 205–234.

462 Mualem, Y., 1976. A new model for predicting the hydraulic conductivity of unsaturated
463 porous media, *Water resources research* **12**(3): 513–522.

464 Nikoosokhan, S., Nowamooz, H. and Chazallon, C., 2015. Effect of dry density, soil texture
465 and time-spatial variable water content on the soil thermal conductivity. geomech geoeng
466 11 (2): 149–158.

467 Nowamooz, H., Nikoosokhan, S., Lin, J. and Chazallon, C., 2015. Finite difference mod-
468 eling of heat distribution in multilayer soils with time-spatial hydrothermal properties,
469 *Renewable Energy* **76**: 7–15.

470 Penner, E., Johnston, G. and Goodrich, L., 1975. Thermal conductivity laboratory studies
471 of some mackenzie highway soils, *Canadian Geotechnical Journal* **12**(3): 271–288.

472 Pike, J., 1964. The estimation of annual run-off from meteorological data in a tropical
473 climate, *Journal of Hydrology* **2**(2): 116–123.

474 Sangi, R. and Müller, D., 2018. Dynamic modelling and simulation of a slinky-coil horizon-
475 tal ground heat exchanger using modelica, *Journal of Building Engineering* **16**: 159–168.

476 Self, S. J., Reddy, B. V. and Rosen, M. A., 2013. Geothermal heat pump systems: Status
477 review and comparison with other heating options, *Applied energy* **101**: 341–348.

478 Shortall, R., Davidsdottir, B. and Axelsson, G., 2015. Geothermal energy for sustainable
479 development: A review of sustainability impacts and assessment frameworks, *Renewable*
480 *and sustainable energy reviews* **44**: 391–406.

481 Tang, F. and Nowamooz, H., 2018a. Hydro-thermal properties of the unsaturated soil,

Civil Infrastructures Confronting Severe Weathers and Climate Changes Conference, Springer, pp. 18–26.

Tang, F. and Nowamooz, H., 2018b. Long-term performance of a shallow borehole heat exchanger installed in a geothermal field of alsace region, *Renewable Energy* **128**: 210–222.

Tang, F. and Nowamooz, H., 2019. Factors influencing the performance of shallow borehole heat exchanger, *Energy Conversion and Management* **181**: 571–583.

Tang, F. and Nowamooz, H., 2020. Outlet temperatures of a slinky-type horizontal ground heat exchanger with the atmosphere-soil interaction, *Renewable Energy* **146**: 705–718.

Turc, L., 1954. The water balance of soils. relation between precipitation, evaporation and flow, *Ann. Agron* **5**: 491–569.

van Genuchten, M. T., 1980. A closed-form equation for predicting the hydraulic conductivity of unsaturated soils, *Soil science society of America journal* **44**(5): 892–898.

Wind, G., 1966. Capillary conductivity data estimated by a simple method, *Technical report*, [sn].

Xu, J., Wang, R. and Li, Y., 2014. A review of available technologies for seasonal thermal energy storage, *Solar energy* **103**: 610–638.

Yoon, S., Lee, S.-R. and Go, G.-H., 2015. Evaluation of thermal efficiency in different types of horizontal ground heat exchangers, *Energy and Buildings* **105**: 100–105.